Elizabeth C. Koeman*, Bruce K. McNamara, Frances N. Smith, Antonio Simonetti and Peter C. Burns

Developing methodologies for source attribution: glass phase separation in Trinitite using NF_3

DOI 10.1515/ract-2016-2641
Received June 8, 2016; accepted October 12, 2016; published online December 19, 2016

Abstract: This study details thermal reactions between glasses, common minerals, and Trinitite post-detonation material with the fluorinating agent nitrogen trifluoride (NF_3). The ultimate goal of our investigation is to develop a relatively rapid method for the effective separation of bomb components from complex matrices resulting from a nuclear explosion. Trinitite samples, silicate minerals (quartz; plagioclase and microcline), amorphous SiO_2, calcite, a natural glass (obsidian), and two synthetic glasses were characterized extensively before and after the fluorination to fully understand the effects of the NF_3 thermal treatment. Samples were reacted with NF_3 using a combined thermogravimetric (TG) differential thermal analysis (DTA) unit, as well as in a stainless steel bomb reactor connected to a fluorination line. Subsequent to the NF_3 treatment, samples were imaged by scanning electron microscopy in order to document changes in grain size and morphology. Energy dispersive spectroscopy was performed to determine changes in major element abundances. Results demonstrate that rates of reaction are dependent on grain size, temperature, pressure, and time of fluorination. All mineral samples experienced mass loss during fluorination. Specifically, amorphous SiO_2 (~90% mass loss) experienced the most while calcite experienced the least (~18%). Major element analysis reveals that mass loss is attributable to the volatilization of silica (SiO_2) in Si-bearing phases, or sample decomposition in calcite due to fluorination. Results for fluorinated samples of Trinitite demonstrate that mass loss occurs at different rates for each sample, but each sample experienced an expected large decrease in Si content (resulting from volatilization of SiF_4). Hence, the concentration of metals in the residual material increased due to the volatilization of Si. These results validate that this thermal-fluorination technique allows the separation of silica from minerals (i. e. naturally occurring crystalline materials) and glasses (i. e. amorphous materials), leaving behind non-volatile fluorinated species and refractory phases. The results from our investigation clearly indicate that the NF_3 treatment of nuclear materials is a technique that provides effective separation of bomb components from complex matrices (e. g. post-detonation samples), which will aid with rapid and accurate source attribution.

Keywords: Nuclear forensics, Trinitite, nitrogen trifluoride, fluorination, glass separation.

1 Introduction

Post-detonation material (PDM) formed from thermal-nuclear bomb detonations will most likely contain fragments from the nuclear device. These remnant materials can include metal components from the housing, detonation electronics, traces of the nuclear core material (including uranium and plutonium), as well as other anthropogenic components. Investigating these bomb-related signatures can lead to source attribution, the ultimate goal of nuclear forensics. PDM from historical nuclear test sites are ideal for developing methodologies for source attribution because information on the device, such as the design and nuclear fuel employed, is known, methodologies can be verified. Trinitite, a historical PDM, has been the focus of previous studies [1–5] because samples are available in the public domain and consist of a relatively simple matrix. In contrast, deciphering the chemical and isotopic signatures for device components within PDMs could be much more complicated and time consuming if the detonation occurs in an urban setting. Therefore, multiple analytical techniques and rapid

***Corresponding author: Elizabeth C. Koeman,** Department of Civil and Environmental Engineering and Earth Sciences, University of Notre Dame, Notre Dame, IN 46556, USA, Tel.: +574-631-5380, E-mail: elizabethkoeman@gmail.com
Bruce K. McNamara and Frances N. Smith: Nuclear Chemistry and Engineering, Pacific Northwest National Laboratory, 902 Battelle Boulevard, Richland, WA 99354, USA
Antonio Simonetti: Department of Civil and Environmental Engineering and Earth Sciences, University of Notre Dame, Notre Dame, IN 46556, USA
Peter C. Burns: Department of Civil and Environmental Engineering and Earth Sciences, University of Notre Dame, Notre Dame, IN 46556, USA; and Department of Chemistry and Biochemistry, University of Notre Dame, Notre Dame, IN 46556, USA

separation analyses may be needed in order to accurately determine the source of a nuclear device.

Trinitite is PDM resulting from the world's first nuclear bomb detonation referred to as the Trinity test. It was detonated on July 16, 1945 at the White Sands Missile Range near Alamogordo, New Mexico (USA). The bomb, named Gadget, was a plutonium implosion device with a Pu core surrounded by a uranium tamper of natural isotope composition [4–6]. Aluminum shells, copper wiring, and other electronics were used in the construction of Gadget [5–7]. Upon detonation from a 30 m tall steel tower, the fireball produced an estimated temperature of at least 8430 K with a duration of 3.1 s [6, 7]. This extremely high temperature melted and vaporized Gadget, the steel tower, and other materials at ground zero (GZ). The end result was the formation of a green, glassy material (Trinitite) that blanketed the area for ~300 m radius from GZ [1].

Trinitite glass not only contains debris and radioactive material from the bomb, as its main constituent is the background geology at GZ. The native material at White Sands Missile Range is arkosic sand dominantly comprised of quartz and feldspars. Other minerals present include: carbonates (e. g. calcite, aragonite, and dolomite), sulfates (e. g. gypsum and selenite), chlorides (e. g. halite and sylvite), clays (e. g. kaolinite and illite), as well as hornblende, olivine, magnetite, ilmenite, and augite [4, 7, 8]. Due to its precursor mineralogy, Trinitite is composed of two types of glasses [8]: 1) a dominantly Si-rich glass from the melting of quartz grains, and 2) a feldspar and clay-based glass. Wallace et al. [9] concluded the quartz-rich glass lacks the radioactive materials from the device (i. e. Pu, U), which are mostly all located within the feldspar and clay melt glass.

The goal of post-detonation nuclear forensics is to find, identify, and ultimately source the bomb components and radioactive material. In previous Trinitite studies, in situ laser ablation inductively coupled mass spectrometry (LA)-ICP-MS was utilized to obtain chemical and isotopic compositions of samples at the micron scale [2, 3, 9–11]. Dustin et al. [12] discusses the comparison between elemental abundance determinations obtained by LA-ICP-MS and bulk digestion methodologies for Trinitite samples, indicating good agreement between both approaches. However, a 'dilution effect' occurs with bulk digestion (analyzed by solution mode-ICP-MS) for Trinitite samples because of the large input of quartz and quartz-rich glass. This effect reduces the concentration of elements of anthropogenic origin from bomb-related materials, and those from the natural background, as quartz does not readily incorporate additional elements into its crystal structure. In order to counteract this dilution phenomenon, this study employs a nitrogen trifluoride (NF_3)-based thermal fluorination technique to remove the silica (SiO_2) from Trinitite. We show this procedure better isolates the anthropogenic bomb-related components for forensic analysis.

Since the Manhattan Project in the early 1940's, fluorination has been applied to nuclear materials. For example, fluorination is used to enrich ^{235}U from uranium ores through gaseous diffusion of UF_6 [13], to separate nuclear materials [14, 15], and platinum metals from irradiated nuclear fuel matrices [16]. Processes involving large-scale fluorination typically depend on using potent fluorinating reagents that are hazardous to human health and the environment (e. g. ClF_3, $BrCl_3$, O_2F_2, HF, and KrF_2 [17]). Moreover, these reagents are generally expensive to produce, ship, and store. The fluorinating agent HF has long been used to separate Si from rocks and minerals [18]; however, this method is time-consuming and as stated above, hazardous. An alternative fluorinating reagent, NF_3, is currently used as a cleaning and etching chemical for microelectronic devices [19–21]). NF_3 is also not corrosive and does not react with moisture, acids or bases at room temperature. More importantly, NF_3 is thermally stable to about 200°C toward most materials and insensitive to shock at pressures of ~100,000 psi [22]. Additionally, NF_3 is nominally non-toxic and thus provides a useful and safer method of screening fluorination behaviors. For comparison, NF_3 is more oxidizing than anhydrous HF, but less aggressive than other fluorinating reagents, such as ClF_3 or F_2 gas [23]. In general, the mechanisms and products of fluorination using NF_3 are most similar to the latter reagents [17]. These properties render NF_3 an attractive reagent for the purpose of silica removal.

In this study, the reactivity of NF_3 is characterized with various synthetic glasses and natural minerals in order to document the effectiveness of Si removal. This methodology is also applied to Trinitite for the purpose of demonstrating its capability of efficiently releasing anthropogenic forensic signatures locked within the melt glass of PDM in a rapid manner of time (hours), compared to well-established, previous radiochemical separation technologies.

2 Experimental methods

2.1 Mineral and glass preparation and characterization

Crystalline mineral and amorphous glass phases were specifically chosen based on differences in their silica

content. Minerals (quartz, K-feldspar, Ca-plagioclase, and calcite) and synthetic glasses (ABCNS-03 and -10) were crushed using a tungsten rock crusher, sieved and split into two size fractions: 45–75 μm and 125–475 μm. Major element compositions for these materials are listed in Table 1. The sample splits were rinsed multiple times with ultrapure water (18.2 mΩ) using an ultrasonicator to remove fines and were subsequently dried overnight in open glass vials in an oven at 105°C. Prior to fluorination, samples were investigated using a scanning electron microscope (Leo SEM, Notre Dame Integrated Imaging Facility) in back-scattered electron (BSE) mode operating with an accelerating voltage of 20 kV. Major element abundances were determined by a Joel JXA-8530F Field Emission electron microprobe at Pacific Northwest National Laboratory (PNNL; Richland, WA, USA). Samples were sputter coated with carbon (10 nm) and analyzed with a beam width of 2 μm, an accelerating voltage of 20 kV, and a beam current of 20 nA. The following well-characterized standards were used for instrument calibration: diopside (Ca, Si), magnetite (Fe), tugtupite (Na, Cl), rutile (Ti), microcline (K), yttrium–aluminum–garnet (Al), rhodenite (Mn), and carbon (C). To further confirm mineral purity, characterization was performed via powder X-ray diffraction (PXRD; University of Notre Dame). A D8 Advanced Davinci (Bruker) PXRD was used to characterize each sample's phase composition with the following parameters: 5–60° 2Θ range, degree step size = 0.02, and a dwell time = 0.5 s/step.

Subsequent to fluorination, samples were fully characterized using the same approaches described above. In order to investigate the effects of fluorination throughout the grains, fluorinated samples were mounted in epoxy and polished to reveal "cross-sectional" views. Images were collected using the Leo SEM and major element compositions were determined by a Cameca SX-50 EMP (University of Notre Dame). The following well-characterized in-house standards were used for instrument calibration: anorthite (Ca, Al, Si), albite (Na), microcline (K), olivine (Fe), rutile (Ti), and calcium fluoride (F). Element maps and BSE images were collected using the Cameca EMP in beam scanning mode with an accelerating voltage of 15 kV and focused beam current of 50 nA. Determination of any phase changes were conducted on the powders using the same PXRD method described above.

2.2 Pre-fluorination Trinitite characterization

Samples of Trinitite were purchased from Mineralogical Research Corporation (www.minresco.com). The samples analyzed in this study were from different groups of Trinitite and were classified based on their morphological features and inclusions. A brief explanation of each sample is provided here: 3 5.25 had a rough, sand-covered bottom surface; 4B 11.59 contained black inclusions; 4C 10.60 consisted of light colored glass/flow marks; 5B 10.22 contained a protuberance on its base; and both TS-1 and TS-2 were interpreted to have formed closest to ground zero (based on ^{152}Eu activities [2]). Trinitite samples were crushed and powdered using a mortar and pestle to a size of < 45 μm and then split into two aliquots; one was fluorinated using a NF_3 thermal treatment and the other was characterized as "unreacted (UR)" samples. Samples were imaged on a Leo scanning electron microscope (SEM) using an accelerating voltage of 20 kV. Major element concentrations of Trinitite powders were collected using energy dispersive spectroscopy (EDS) for each sample, with associated relative uncertainties of ±10% (2σ). Trinitite powders were dissolved in a HF : HNO_3 acid mixture (4 : 1 ratio) in closed 15 mL Savillex® Teflon beakers on a hot plate at ~120°C for 48 h. Samples were then uncapped, dried down, and fluxed twice in concentrated HNO_3 acid within capped Teflon beakers for a period of 24 h (each cycle). These samples were then dried down, re-dissolved in concentrated nitric acid and subsequently diluted to a final volume of 100 mL with ultrapure (18 MΩ) water. Trace element abundances were determined using

Table 1: Major element compositions of mineral, natural glass, and synthetic glass samples obtained by EMP (wt%).

	SiO_2	Al_2O_3	CaO	K_2O	Na_2O	TiO_2	FeO	MnO	CO_3	Total
Quartz	99.98									99.98
Plagioclase	63.78	21.44	3.05	0.22	11.48		0.03			100.0
K-feldspar	64.45	18.40		16.53	0.93		0.01			100.2
Obsidian	80.19	11.43	0.27	4.98	0.63	0.48	1.90	0.06		99.94
Calcite			57.09						42.89	99.98
ABCNS-03	68.74	19.44			11.82					100.0
ABCNS-10	52.21	22.15	12.18		13.46					100.0

a standard/spike addition method [24] on a ThermoFinnegan Element2 sector-field high resolution (HR)-ICP-MS.

A detailed comparison between elemental abundances obtained by LA-ICP-MS analyses from thin sections and those for reacted powders from the same (bulk) Trinitite sample is presented in Dustin et al. [12]; a similar approach was adopted here. Laser ablation analyses were conducted with an ESI-New Wave Research UP-213 laser ablation unit coupled to the Element2 (HR)-ICP-MS. Background ion signals were collected for 60 s with the laser on and shuttered, followed by 60 s of ion signal collection. A 'standard-sample' bracketing technique was employed with analyses of the NIST SRM 612 international standard glass wafer to monitor for instrumental drift [25]. Electron microprobe analysis was used to determine the CaO wt% in each area analyzed and this value was used as an internal standard.

2.3 Direct monitoring fluorination approach

Trinitite powders, minerals, and glasses were fluorinated at PNNL. Reactions of NF_3 with various minerals were performed in two general ways. In one method, a Seiko (model 350) thermogravimetric analysis (TGA) and simultaneous differential thermal analysis (DTA) unit, modified to accommodate NF_3 flow through with an inert carrier gas (e. g. argon or nitrogen), was used to monitor reactions with duration lasting 1–2 h. A full description of the instrumentation and method used here is reported in [17]. In short, samples weighing 10–20 mg were loaded into aluminum pans (99.999% Al; RT Instruments, Woodland, CA, USA) that were pretreated for 1 h with NF_3 at 500°C at a ramp rate of 50°C/min. This step was to passivate the pan surfaces, as well as to ensure that their fluorination during subsequent TG/DTA analyses did not cause any small mass changes [17]. Samples were heated in isothermal mode to different temperatures (> 500°C) followed by the input of NF_3 gas. Mass (TG) and heat flow (DTA) baselines were collected under the same conditions.

Unfortunately, the corrosive nature of the reactions often precluded the use of such online monitoring approaches. Although NF_3 is a mild fluorinating reagent near ambient temperature, its reactivity at temperatures at 550°C or above corrodes the internal parts of the thermal gravimetric instrument over extended exposures. Consequently, several reactions are not reported by this method. Rather, the extent of the reaction from static bomb exposures was interpreted by bulk mass changes and investigation of the products after fluorination.

2.4 Static fluorination approach

The second method for fluorination of Trinitite powders, minerals, and glasses at PNNL was using a static bomb on a fluorination line (Figure 1). The samples were loaded in an Al pan housed within a 2 cm Monel cylinder with a filter to allow the passage of gas in and out of the sample container. The Monel cylinder was loaded into a stainless steel chamber attached to a vacuum line through a flange disconnect. The Monel vacuum line was connected to a gas manifold that allowed admission of pressures of UHP argon (Oxarc), 99.99% NF_3, or 10% fluorine gas in argon (Air Liquide). An insulated heater jacket placed around the static bomb was used to heat mixtures of these gasses with mineral and glass samples. After the container was evacuated of air, approximately 1 atmosphere of NF_3 was added at room temperature. After the admission of NF_3, mineral and glass samples were allowed to react for 1–2 h within the sample chamber at 500°C, cooled and subsequently weighed for mass loss. To determine if a particular condition resulted in complete reaction, the reacted sample was split, then one half was reacted using the same procedure for a total 2 h reaction period.

2.5 Post-fluorination sample characterization

Reacted samples were imaged and major element abundances were determined using the same instruments and methodology described above (SEM/EDS). Trinitite samples were digested using the same procedure detailed previously for the determination of trace element concentrations. For measurement of U and Pu

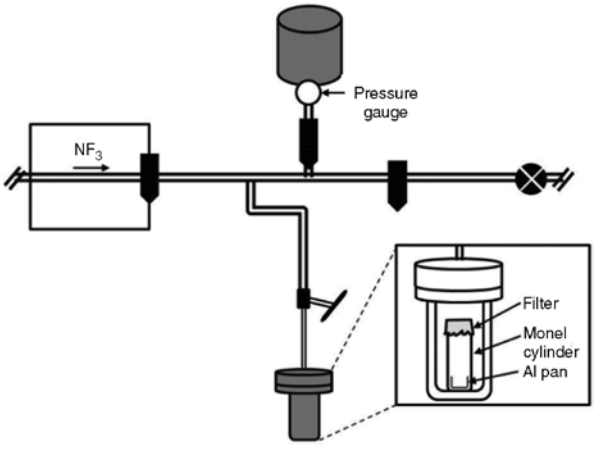

Figure 1: Schematic of static fluorination line apparatus at Pacific Northwest National Laboratory.

isotope compositions, 14 mL aliquots were taken from the 100 mL solution containing the digested samples, and these were dried down in 15 mL Savillex® Teflon beakers so as to increase their concentrations (and hence their respective ion signals) in the final sample solutions. Once dry, the material was re-dissolved in 5 mL of 2% HNO_3. Thallium (10 ppb) was added to the sample solutions as an internal standard and used to monitor and correct for instrumental drift. Solutions were then analyzed using a Nu Instruments AttoM high resolution inductively coupled plasma mass spectrometer (HR-ICP-MS). Uranium abundances were determined by an external calibration method by analyzing a set of known uranium concentration calibration solutions (0.1 ppb, 0.5 ppb, 1 ppb, 2 ppb, and 5 ppb) followed by the fluorinated Trinitite samples. The U calibration solutions yielded the following correlation coefficients: $^{238}U = 0.9998$ and $^{235}U = 0.9948$. Due to the lack of a plutonium standard solution, the calibration for ^{238}U was used to determine the abundances for $^{239,240}Pu$; this assumption is valid as the ion yields for U and Pu are similar due to their almost equivalent atomic masses.

3 Results

3.1 Mineral and glass results

Major element compositions of all unreacted minerals and glasses obtained by EMP are listed in Table 1. Examples of TG/DTA thermal scans of the reaction of 10% NF_3 in argon with quartz (both size fractions) and calcite demonstrate different reactions and mass loss over time (Figure 2). To further investigate these reactions, larger sample sizes were reacted in the fluorination line (Figure 1). Subsequent to reaction with NF_3, each sample was weighed, the percent mass loss was calculated and normalized to the original SiO_2 wt% of each sample (Table 2). When samples were normalized to their original respective SiO_2 wt% values, it showed amorphous SiO_2 experienced the most significant mass change, followed in order of decreasing change by ABCNS-03, K-feldspar, plagioclase, obsidian, quartz, ABCNS-10, and lastly calcite. SEM/BSE images of reacted powders demonstrate that the fluorination caused important morphological changes to each sample (Figure 3). Figure 4 displays PXRD patterns for quartz, K-feldspar, plagioclase, and calcite in all the stages of the experiments (unreacted and fluorinated). These patterns demonstrate the lack of noticeable phase changes that occurred due to fluorination of quartz, but new peaks

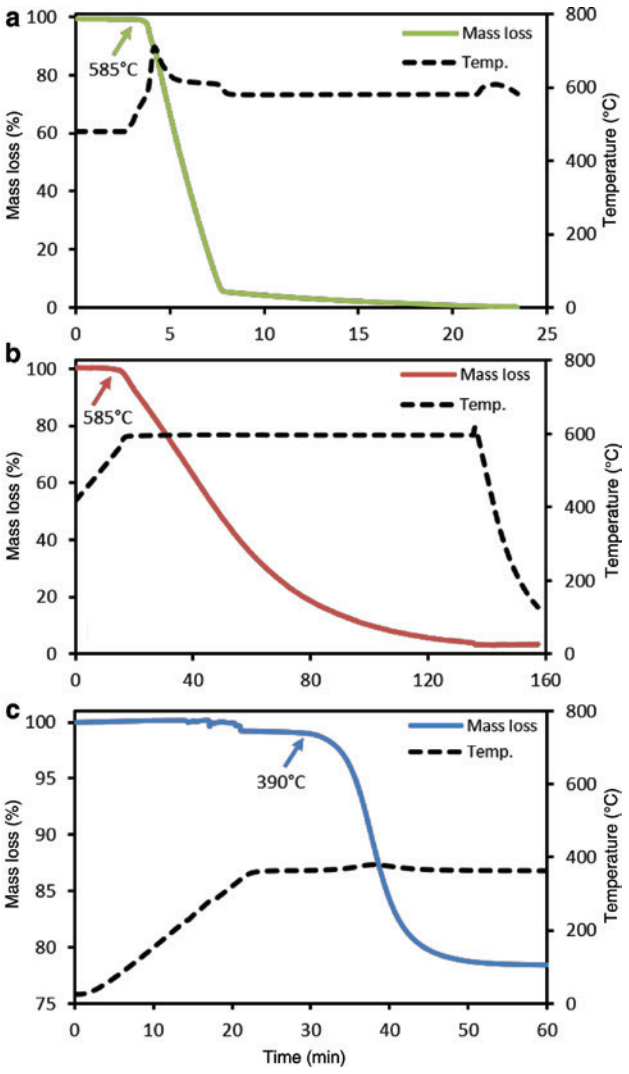

Figure 2: Thermal scans measured via TG/DTA for (a) 45–75 µm quartz, (b) 125–475 µm quartz, and (c) 45–75 µm calcite; note different x-axes. Arrows point to the time and temperature each sample began reacting with NF_3. Also note the runs are isothermal, but some samples needed a higher temperature to facilitate reaction (e. g. sample a).

are visible in the patterns for K-feldspar, plagioclase, and calcite (Figure 4).

SEM and EMP images of epoxy-mounted samples reveal that fluorination affects each sample differently. Whereas the glasses (obsidian, ABCNS-03 and-10) have noticeable rims surrounding the grains, quartz grains lack reaction rims but are characterized by diffuse outlines. Plagioclase and K-feldspar also exhibit rims, but alterations can be seen along their cleavage planes. EMP elemental maps (Supplementary Information) and point analyses (Figure 5, Table 3) reveal these reaction rims/areas are dominantly composed of F, K, Al and lack Si. It

Table 2: Reaction parameters and mass loss for samples (125–475 μm size fraction) studied here.

Sample	Pressure (NF_3; torr)	Temp (°C)	Fluorination duration (h)	Starting mass (mg)	Final mass (mg)	Mass loss (%)	Mass loss %/ SiO_2 wt% (%)
Amorphous SiO_2	932	520	1.5	74.9	7.9	89.5	89.5
Quartz (1)	929	440	2	126.7	104.3	17.7	17.7
Quartz (2)	925	440	3	112.6	70.4	37.5	37.5
Plagioclase (1)	830	550	2	126.3	81	35.9	56.3
Plagioclase (2)	830	450	3	141.9	107.6	24.2	37.9
K-feldspar (1)	840	500	2	268.0	220.0	17.9	27.8
K-feldspar (2)	820	550	2	98.4	59.4	39.6	61.4
Calcite	820	400	2	76.3	62.4	18.2	–
Obsidian (1)	407	400	1	57.2	47.7	16.6	20.7
Obsidian (2)	632	550	2	81.9	46.7	43.0	53.6
ABCNS-03 (1)	933	460	2.5	107.8	62.0	42.5	61.8
ABCNS-03 (2)	934	570	2	127.4	61.9	51.4	74.8
ABCNS-10 (1)	954	550	2	114.0	84.0	26.3	50.4
ABCNS-10 (2)	944	425	1.5	125.1	104.9	16.1	30.8

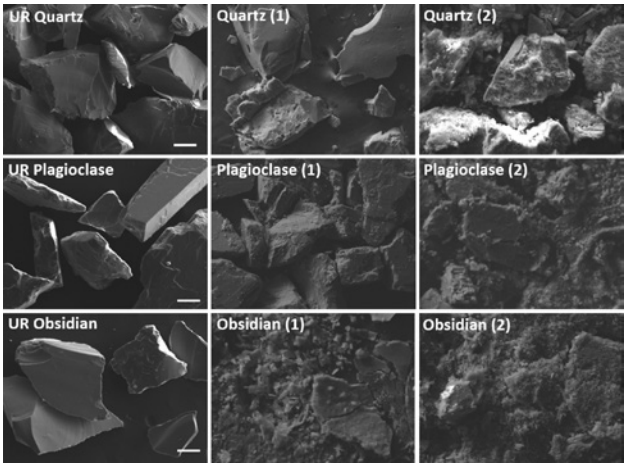

Figure 3: SEM/BSE images of unreacted (UR) quartz, plagioclase, and obsidian. Reacted samples are labeled and fluorination conditions can be found in Table 2. Scale bars are 100 μm and apply to each image.

is important to note that the EMP analyses of the reacted areas do not total to 100%. Further investigations of these areas using μ-XRF demonstrate the missing element mass may be attributed to fluorine (Supplementary Information).

3.2 Trinitite results

The amount of mass loss for each Trinitite sample due to fluorination is listed in Table 4, and in general the values range between 39 and 66%. Trinitite samples also experienced color changes due to fluorination; powdered Trinitite samples (UR) are gray in color and reacted samples turned pink, brown, and orange with increasing fluorination. Fully reacted samples (no further mass loss) turned white. This progression of color changes occurred for all Trinitite samples, but not for the synthetic glasses. Scanning electron images document the large morphological changes that samples undergo during fluorination (Figure 6). For example, whereas unreacted (UR) TS-2 still contains large pieces of Trinitite (~250 μm; Figure 6), subsequent to fluorination for 1 h the grain size decreases significantly (< 150 μm). This reduction in grain size is even more evident after the 2 h fluorination (< 100 μm; Figure 6). Average major element concentrations for samples investigated here are listed in Table 5. These analyses demonstrate that for each sample, the silica content decreases after each thermal treatment with NF_3.

Trace element concentrations (determined by Solution Mode (SM)-ICP-MS) for UR and fluorinated samples are provided in the Supplementary Information. These are also plotted in Figure 7 in which the abundances for reacted samples are normalized to those corresponding for the UR sample (SM). A normalized value of 1 (shown as a solid black line) indicates that both UR and reacted samples have the same concentration (for any element). The dashed vertical lines within plots point to elements of interest, which are characterized by large deviations from unity: U, Co, Cu, and Pb (Figure 7). The trace element patterns for each sample are very similar, recording the same positive and negative anomalies. Furthermore, the 2 h reactions are characterized by higher (e. g. U, Co, Cu) concentrations compared to the 1 h samples.

Metals that are interpreted to be of anthropogenic origin (Pb, Cu, Co) are plotted in Figure 8. These reveal

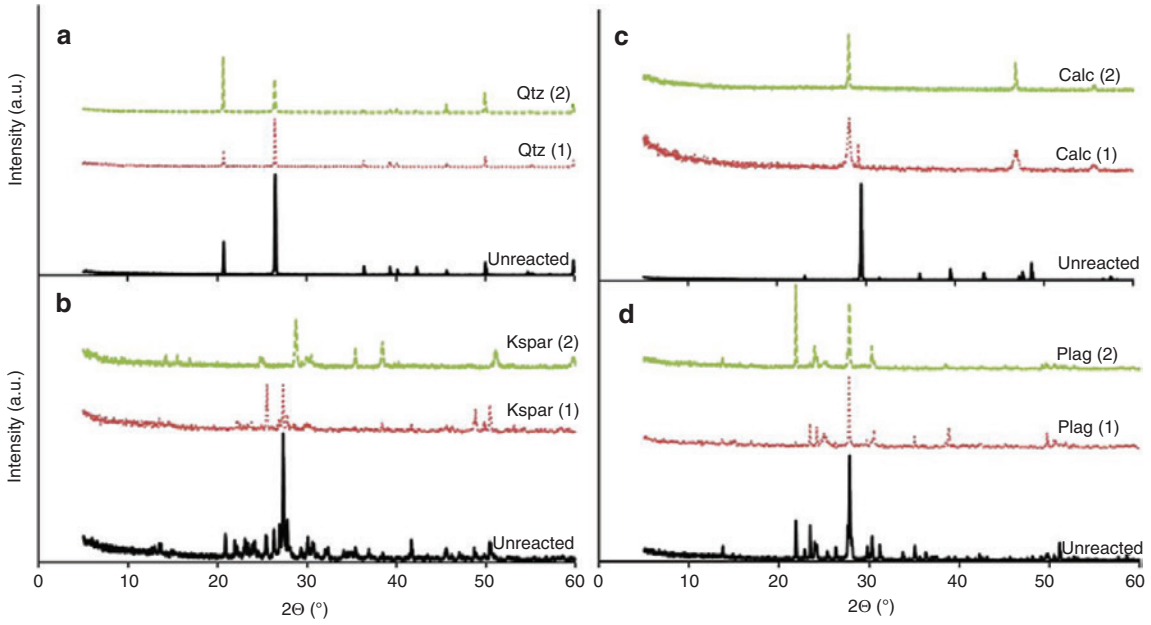

Figure 4: Powder X-ray diffraction (PXRD) patterns for (a) quartz, (b) K-feldspar, (c) calcite, and (d) plagioclase. The patterns for fluorinated samples are also displayed and labeled accordingly. Fluorination conditions are listed in Table 2.

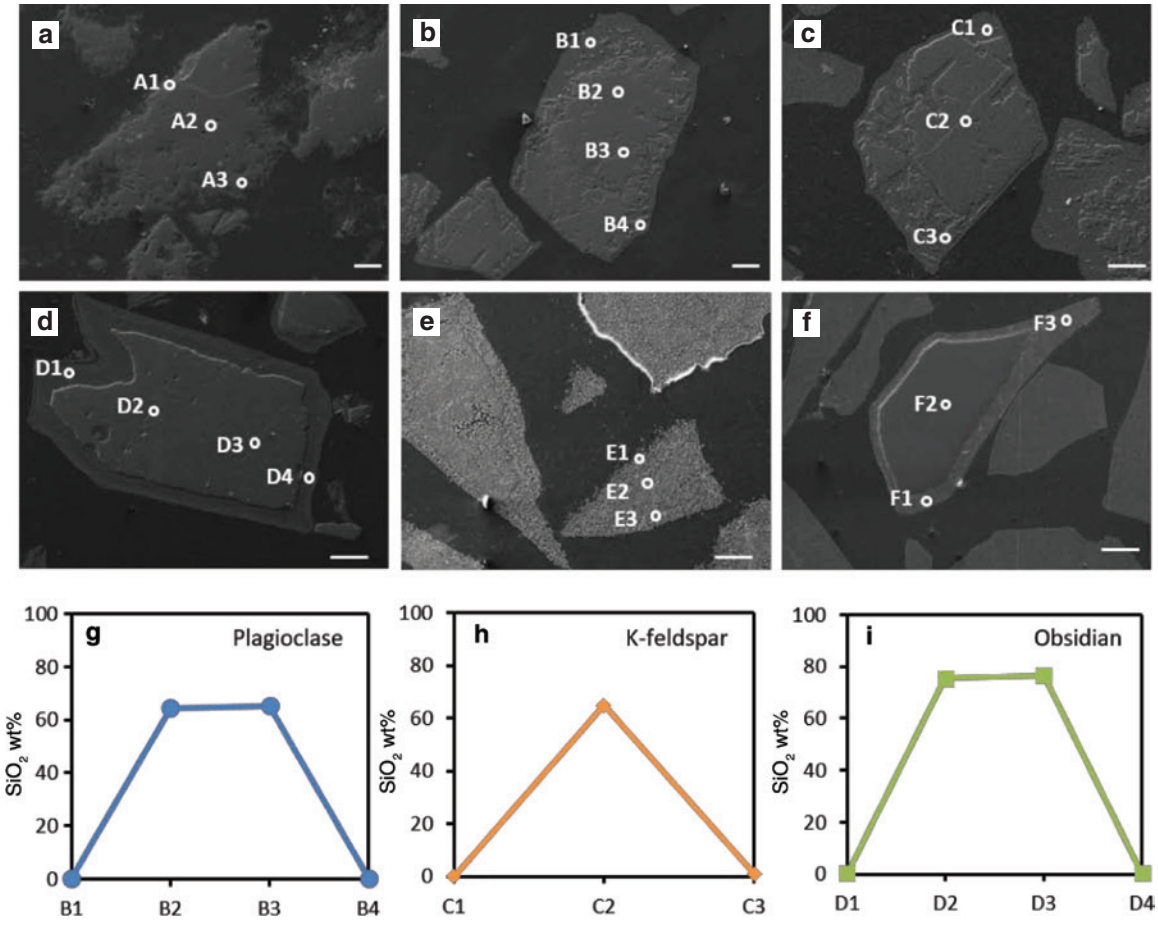

Figure 5: SEM images of (a) quartz (2), (b) plagioclase (2), (c) K-feldspar (2), (d) obsidian (2), (e) ABCNS-03 (2) and (f) ABCNS-10 (2). Spot analyses are listed in Table 3 and all scale bars are 50 μm. Graphs G-I are SiO_2 (wt%) concentration profiles of select samples.

Table 3: Major element compositions of reacted minerals shown in Figure 5.

Sample	Label	SiO_2	Al_2O_3	CaO	K_2O	Na_2O	TiO_2	FeO	Total
Quartz	A1	87.19							87.19
	A2	98.77							98.77
	A3	89.75							89.75
Plagioclase	B1	0.23	39.17	2.87	5.38	11.21		0.82	59.68
	B2	64.57	22.56	2.78	0.46	9.76		0.02	100.2
	B3	65.37	22.38	2.98	0.32	9.98		0.05	101.1
	B4	0.23	36.95	3.23	1.52	9.75		0.17	51.85
K-feldspar	C1	0.06	31.80		22.78	0.75			55.39
	C2	64.93	18.65		15.72	0.63			99.93
	C3	1.13	31.93		26.25	0.69		0.04	60.04
Obsidian	D1	0.49	20.20	0.41	6.07	6.55	0.21	2.85	36.78
	D2	75.6	12.01	0.26	5.11	2.61	0.12	1.84	97.55
	D3	76.63	12.02	0.23	4.67	3.01	0.09	1.79	98.44
	D4	0.49	20.40	0.39	6.84	6.33	0.24	2.78	37.47
ABCNS-03	E1	0.97	31.49		0.05	14.03			46.54
	E2	0.74	34.12		0.10	9.96			44.92
	E3	0.09	29.64		0.06	7.88			37.67
ABCNS-10	F1	0.24	29.25	17.08	0.01	15.89			62.47
	F2	52.24	21.89	12.27	0.01	5.58			91.99
	F3	0.25	32.70	17.48	0.03	17.62			68.08

Table 4: Mass loss for Trinitite samples investigated in this study.

Sample	Starting mass (mg)	Final mass (mg)	Mass loss (%)
3 5.25 (1 h)	141.9	55.3	61
3 5.25 (2 h)	38.1	15.7	59
4B 11.59 (1 h)	145	72.7	50
4B 11.59 (2 h)	38.7	15.5	60
4C 10.60 (1 h)	220.2	79.1	64
5B 10.22 (1 h)	136.5	59.5	56
5B 10.22 (2 h)	38.1	12.8	66
TS-1 (1 h)	96.4	58.7	39
TS-1 (2 h)	30.5	14.4	53
TS-2 (1 h)	159	123	23
TS-2 (2 h)	68.1	36.9	46

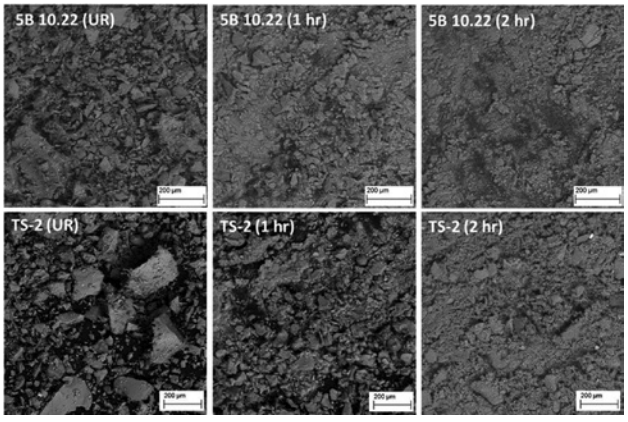

Figure 6: Scanning electron images of samples 5B 11.59 and TS-2 at each stage (unreacted, fluorinated for 1 h, and 2 h).

Table 5: Major element concentrations (wt%) of UR and reacted samples of Trinitite.

Sample	SiO_2	Al_2O_3	CaO	K_2O	Na_2O	FeO
3 5.25 (UR)	76.4	10.9	7.4	5.3	0.0	0.0
3 5.25 (1 h)	21.0	27.6	29.8	21.6	0.0	0.0
3 5.25 (2 h)	5.7	31.2	31.8	19.4	11.9	0.0
4B 11.59 (UR)	73.3	9.4	8.2	7.5	0.0	0.0
4B 11.59 (1 h)	13.8	27.1	21.7	22.5	0.0	15.0
4B 11.59 (2 h)	0.0	28.7	28.7	27.5	0.0	15.2
5B 10.22 (UR)	72.8	15.9	5.7	2.1	1.2	1.9
5B 10.22 (1 h)	17.4	33.2	22.3	16.8	0.0	3.4
5B 10.22 (2 h)	2.4	35.3	30.2	20.5	0.0	9.7
TS-1 (UR)	73.4	8.8	7.1	4.8	2.2	3.8
TS-1 (1 h)	18.2	32.3	24.5	16.7	0.0	8.3
TS-1 (2 h)	0.0	45.6	23.3	18.2	0.0	12.1
TS-2 (UR)	72.0	13.6	2.9	6.0	0.9	1.5
TS-2 (1 h)	26.5	21.1	19.8	17.1	3.7	5.2
TS-2 (2 h)	1.2	28.4	28.5	23.5	6.3	10.8

that the UR solution mode (SM) analyses fall within the largest grouping of in situ (unreacted LA of thin sections) analyses for the same samples. This result further corroborates the main conclusions reported in Dustin et al. [12] in relation to the significant match between bulk solution mode analyses and median elemental concentration determinations based on LA-ICP-MS analyses for identical samples. The data shown in Figure 8 also demonstrate that reacted samples have higher amounts of

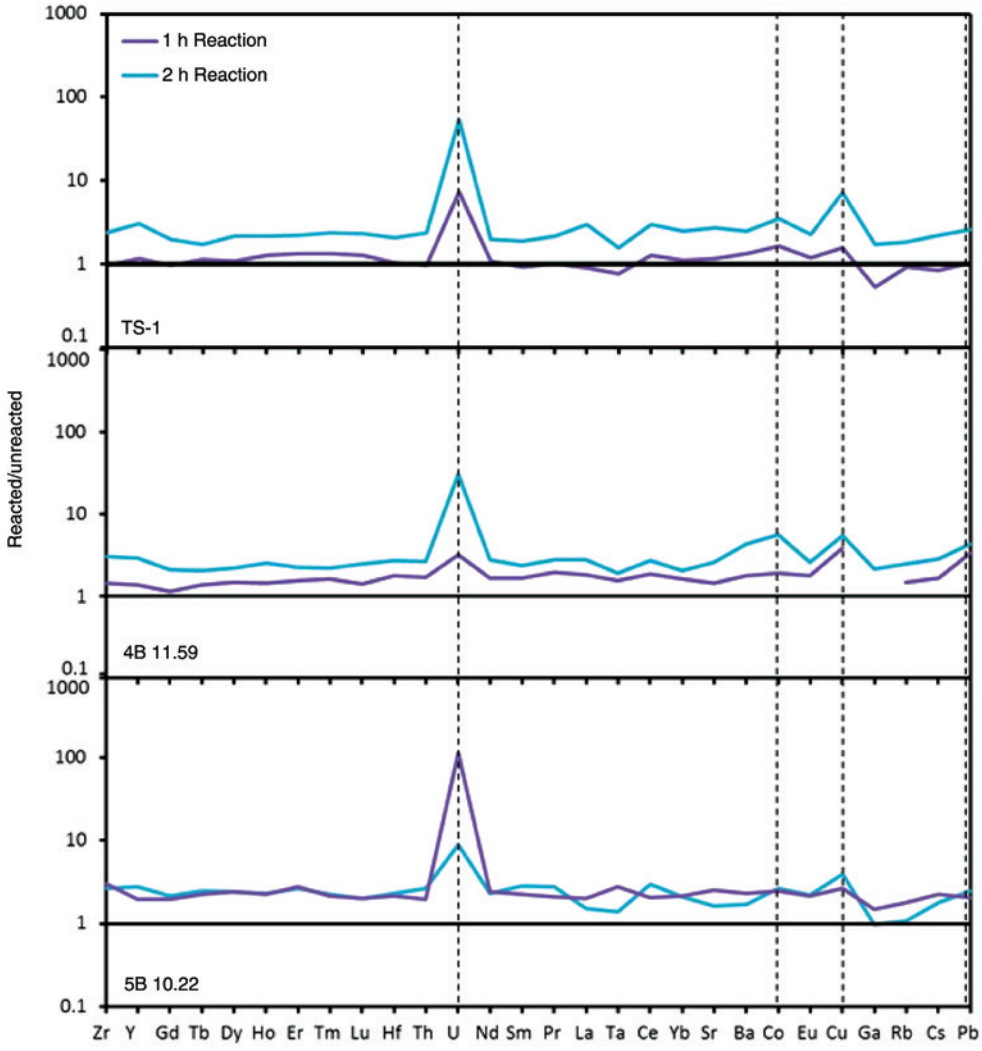

Figure 7: Reacted samples normalized to UR (log scale). Plots are labeled by sample and legend in top diagram applies to each plot.

metals relative to their respective UR samples. Chondrite normalized diagrams are commonly used to compare REE abundances in samples to those in solar system abundances so as to eliminate the Oddo–Harkins effect and hence facilitates the identification of chemical fractionations. In this case, the chondrite normalized diagrams indicate that reacted samples are enriched in REEs relative to the UR sample and generally have the same patterns (Figure 9), which suggests that the NF_3 treatment did not change/fractionate the relative proportion of the REEs.

Uranium concentrations generally increase with duration of fluorination (Figure 10a); however, two samples (3 5.25 and 5B 10.22) contain similar U concentrations in both the 1 and 2 h reactions. Figure 10b reveals Pu concentrations also increase after 1 h, but either remained constant or decreased after the second hour of fluorination. Of utmost importance, almost all of the measured $^{240}Pu/^{239}Pu$ ratios for the fluorinated samples are consistent with previously reported values for Trinitite as shown in Figure 11 ($^{240}Pu/^{239}Pu \approx 0.020–0.030$; [3, 5, 9, 12, 26]).

Of note, subsequent completion of most of the work reported here, it was determined that samples of UO_2 fluorinated by NF_3 in the static reaction apparatus were not in their hexavalent state. In separate experiments, however, hexavalent fluorides were formed in a purely Monel apparatus and in all TGA experiments. The reactions of SiO_2 to SiF_4 clearly were observed in the stainless steel bomb. This would indicate that the stainless steel apparatus in some manner did not allow oxidation of uranium or plutonium to the hexavalent state. Therefore, the uranium and plutonium in the Trinitite samples could not be volatilized in the stainless apparatus.

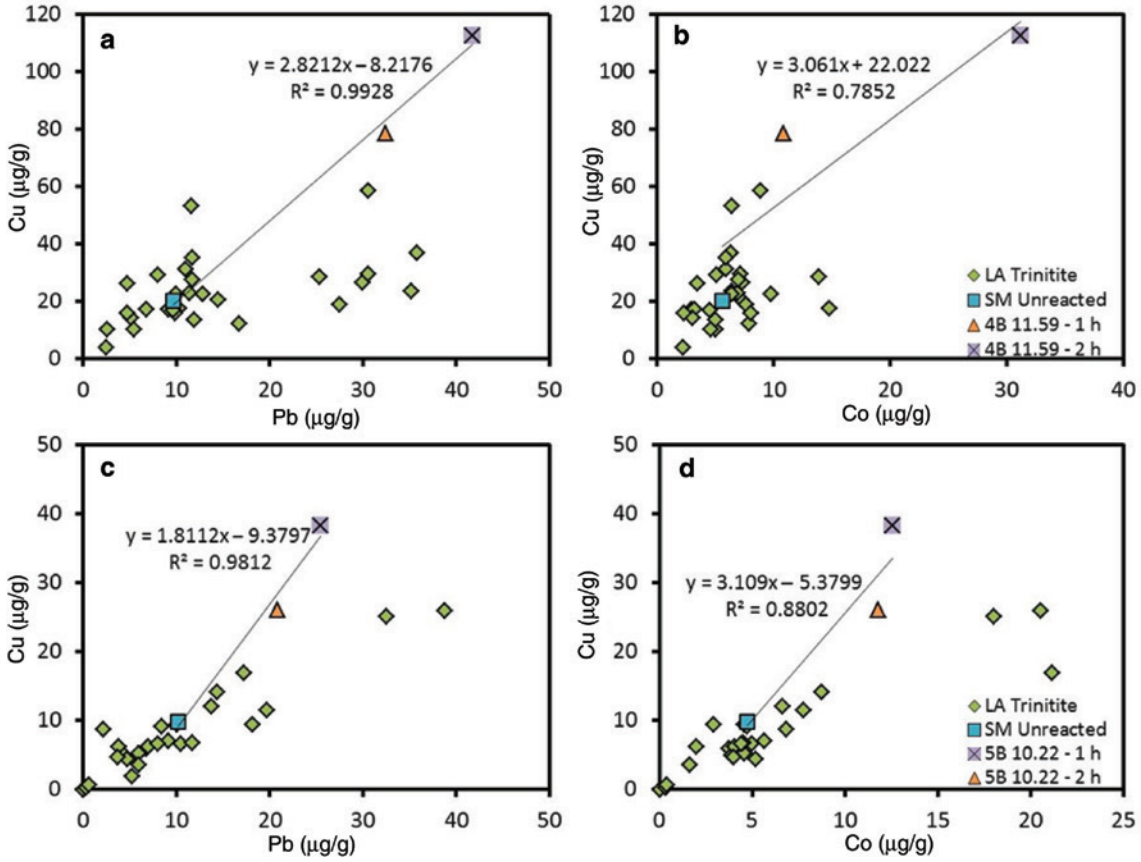

Figure 8: (a) Cu vs. Pb and (b) Cu vs. Co for 4B 11.59 (legend in a also applies to a). (c) Cu vs. Pb and (d) Cu vs. Co for 5B 10.22 (legend in d also applies to c).

4 Discussion

In the instances that TGA can be used, mass loss due to volatilization is a useful probe of mineral and glass degradation during fluorination. Thermal scans of the reaction of 10% NF_3 in argon with quartz (both large and small-size fractions) and calcite (small-size fraction) demonstrate differences in onset temperature and mass loss (Figure 2). Calcite reacted with NF_3 (began experiencing mass loss) at the lowest temperature (390°C; Figure 2c). Both quartz size fractions reacted at the highest temperature (585°C) and lost most of their initial weight (Figure 2a–b). The mass loss in both quartz samples can be explained by the reaction shown in Eq. 1; Si volatilizes with the fluorine gas, thus leaving the sample. In the case of $CaCO_3$, the mass gain by addition of fluorine to make CaF_2 is shown in Eq. 2. Theoretical mass loss (~18 wt%; Table 2) was observed for this reaction. The completion of the reaction shown in Eq. 2 is evidenced in the PXRD patterns for the reacted calcite since the unreacted sample was verified as calcite, whereas peaks for both reacted samples correspond to those for CaF_2 (Figure 4c).

$$SiO_2 + 4/3NF_{3(g)} = SiF_{4(g)} + 2/3N_{2(g)} + O_{2(g)} \quad (1)$$

$$CaCO_3 + 2/3NF_{3(g)} = CaF_2 + CO_{2(g)} + N_2 + 1/2O_{2(g)}. \quad (2)$$

The impact of particle size on the thermal profile is demonstrated for quartz (Figure 2a–b). The smaller particle size material (45–75 µm; Figure 2a) reacted fairly rapidly, whereas the large size fraction (125–475 µm; Figure 2b) was kinetically slow to react even though the mass loss initiated at the same temperature (585°C) for both particle sizes. This result demonstrates particle size exerts a significant control on the rate of degradation for the same material.

The time and temperature of fluorination, as with particle size, have large impacts on the rates of sample degradation. Table 2 lists all fluorinated samples with their corresponding times and temperatures of reactions. Two samples of quartz were run using the same conditions (temperature, pressure, and similar starting masses) except for fluorination time. Quartz (1) was allowed to react for 2 h while quartz (2) was reacted for 3; the latter lost ~20% more weight. When all the conditions are constant but

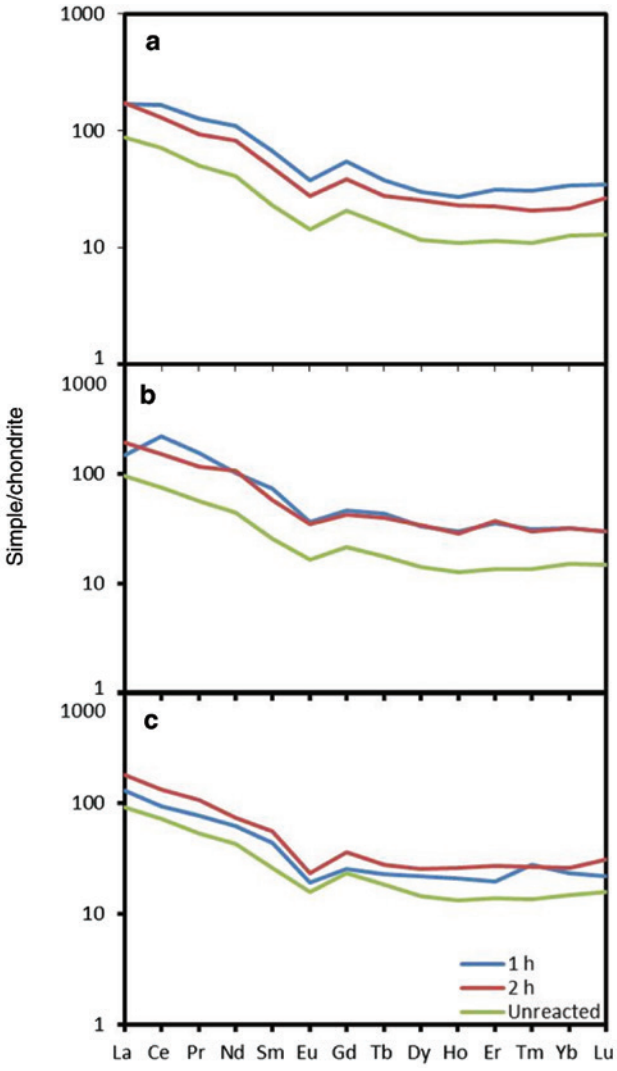

Figure 9: Chondrite normalized REE plots comparing UR and reacted samples for (A) 3 5.25, (B) 5B 10.22, and (C) TS-2. Legend in C applies to all plots. Chondrite values are taken from McDonough and Sun [30].

temperature is increased, the higher temperature reaction allows for more mass loss. This is evident in plagioclase, K-feldspar, obsidian, and both synthetic glasses (Table 2). These results indicate that temperature has a greater effect on mass loss than reaction time.

Although time, temperature, and particle size affect the amount of sample material being fluorinated, it is clear that all samples are experiencing significant mass loss and degradation (Figure 3; Table 2). EMP and PXRD analyses indicate that this mass loss is occurring due to the volatilization of Si, with the exception of calcite (Eqs. 1 and 2; Table 3). The elemental map for quartz indicates Si is being removed from the sample (Supplementary Information), while the PXRD patterns for the reacted samples do not contain any evidence for the formation of secondary phases and still contained peaks for quartz. This indicates that the Si is being volatilized with F in the form of SiF_4 (Eq. 2) but the reaction did not go to completion. Plagioclase (Figure 5b), obsidian (Figure 5d), and K-feldspar (Figure 5c) also lose Si and a fluorine rich rim is produced at the grain boundaries. Compositions listed in Table 3 indicate that the rims are enriched in Al_2O_3 and K_2O relative to their unreacted counterparts. When comparing the minerals/glasses directly against each other, amorphous SiO_2 was the most reactive to NF_3 and calcite the least (due to calcite not containing Si). Interestingly, K-feldspar and plagioclase were more reactive than quartz, even though the feldspars have less SiO_2 wt% than quartz (Table 1). This could be due to the fact that quartz does not have cleavage planes while the feldspars do; an increased level of reactions with NF_3 can be seen along the cleavage planes of K-feldspar and plagioclase (Figure 5b–c and Supplementary Information).

In addition to volatile fluorinated phases that lead to mass loss, refractory fluorine phases also arise and

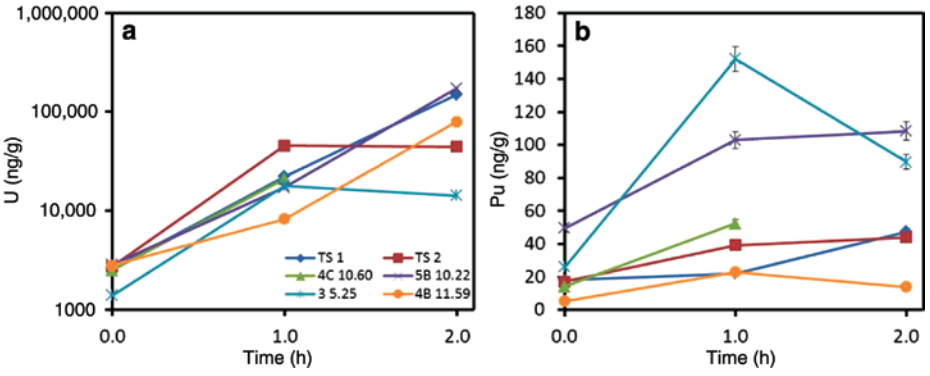

Figure 10: Uranium (a) and Pu (b) concentrations for UR (0 h), 1 and 2 h reactions. Legend in a applies to both plots. Error bars in (b) are 2σ.

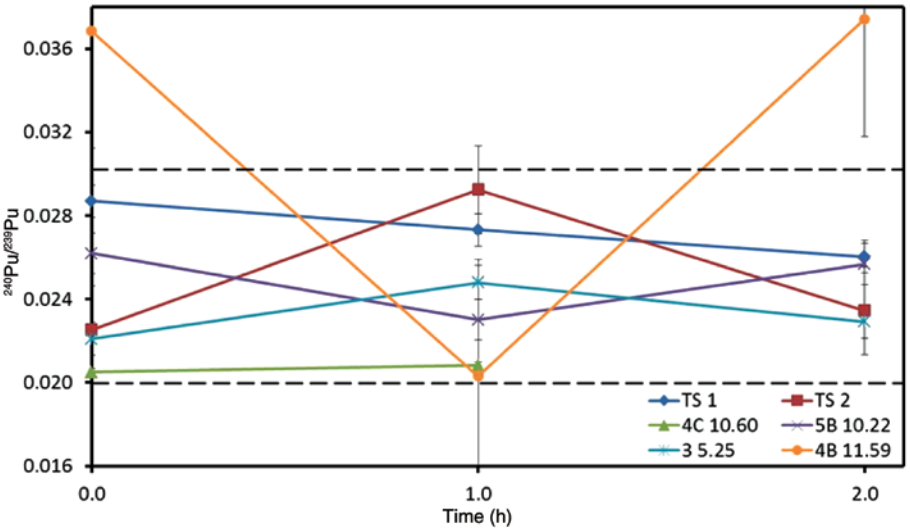

Figure 11: Plutonium isotope ratios for each sample vs. fluorination time (UR = 0 h). The dashed lines represent range of $^{240}Pu/^{239}Pu$ isotope ratios for Trinitite previously reported in the literature [3, 5, 9] Error bars are 2σ.

can be detected experimentally. PXRD patterns reveal the occurrence of fluorine phases within these samples, much like with calcite (CaF_2; Figure 4c). While the first reacted plagioclase sample still contains peaks matching its mineral form, the second reacted sample includes peaks corresponding to AlF_3 (Figure 4d). Reacted K-feldspar samples also contain peaks matching its mineral form, as well as the fluorine compound $KAlF_4$ (Figure 4b). Although fluoride-bearing compounds are being produced with elements that are not volatile, EMP analyses confirm that the fluorination of samples is volatilizing Si (Figure 5; Table 3).

Similar morphological changes occurred with Trinitite samples compared to minerals and glasses. The morphology of UR and reacted Trinitite samples are shown in Figure 6. The SEM images demonstrate Trinitite experienced degradation during fluorination, likely from the removal of Si. Major element compositions of samples (Table 5) indicate that the UR Trinitite samples contain 72–77 wt% SiO_2 (from relict quartz grains, and both quartz and feldspathic glasses). Subsequent each reaction with NF_3, SiO_2 contents (wt%) decrease significantly (down to 14–27 wt% after 1 h reaction); this is due to the production of gaseous SiF_4 (Eq. 1).

The removal of Si from Trinitite samples during fluorination reduces the 'dilution effect' described in Dustin et al. [12], and therefore allows for the enrichment of trace element concentrations (Figures 7–10). Trace metals previously determined to be of anthropogenic origin (e. g. Co, Cu, Pb; [4, 7, 11, 27]) are therefore important to identify. The sand at GZ contains ~ 26 µg/g of Cu while 'green' Trinitite can contain between 2.6 and 312 µg/g Cu [11]. The Trinitite samples investigated here have Cu concentrations within this range. After treatment with NF_3, all samples are characterized by higher amounts of Cu (Figure 7; Supplementary Information). Both Pb and Co also record increases in their respective abundances (Figures 7 and 8). More importantly, the ratio between Pb and Cu remains relatively constant from UR to reacted samples, implying they originate from the same source [10, 28]. This further validates the enrichment in reacted samples as being device related.

Identification of U in Trinitite or other PDMs is also significant because it can be used as fuel, or in this case, as a tamper [6]. The tamper used in Gadget was composed of 120 kg of natural U, and after detonation the U was dispersed and incorporated into the Trinitite melt glass [6]. However, part of the U found in Trinitite can be attributed to natural U-bearing minerals found in the sand at GZ (e. g. zircon, monazite, and apatite [8, 11]). The sand contains an average U concentration of ~ 3.2 µg/g [11]; this is comparable to U concentrations determined for UR Trinitite investigated here. Despite these low concentrations, the fluorinated samples are characterized by elevated abundances of U (Figure 8; Supplementary Information). For example, unreacted sample TS-1 contains ~ 2.3 µg/g of U and after the 2 h reaction, the concentration increased to ~ 124 µg/g (Figure 10a). In situ LA-ICP-MS analysis of this sample also records high abundances of U (~ 35 µg/g); this value is particularly close to the maximum U concentration found in 'green' Trinitite (~ 45 µg/g [11]).

While deciphering the chemical signatures of all device-related components is of importance, identifying

the type of fuel is a priority because its isotope composition is dependent on age and fuel cycle used. The Pu isotopic composition of the fuel used in the Trinity device is known; however, development of a methodology to determine the Pu isotope ratios of future PDMs is critical since the isotope composition of the nuclear device will most likely be unknown (prior to detonation). Dustin et al. [12] discussed the correlation between ion signal (counts) of ^{239}Pu and ^{240}Pu/^{239}Pu ratios obtained by LA-ICP-MS; the measurements indicate that analyses recording higher ion signal intensities (>1000 cps) of ^{239}Pu yield bomb-related Pu signatures (^{240}Pu/^{239}Pu ≈ 0.020–0.030) close to the calculated Trinity Pu isotope composition (^{240}Pu/^{239}Pu ≈ 0.013 [5]). Additionally, the results reported indicate that caution must be used when assessing the Pu isotope composition of PDMs since analyses of Trinitite characterized by much lower ion signal intensities (<1000 cps) tend to yield higher ^{240}Pu/^{239}Pu ratios (between 0.030 and 0.20); this would naturally lead to a false Pu isotope signature determination for the nuclear device [26].

In this study, samples treated with NF_3 yielded ^{239}Pu ion signal intensities between ~5500 and 99,800 cps (^{240}Pu ≈ 120–2400 cps). The Pu abundances for the NF_3 treated samples were determined using an external calibration curve for U due to the lack of a Pu standard. Figure 10b displays the Pu concentrations of UR Trinitite; these range between 5.3 and 49.6 ng/g and abundances of Pu increased between 20 and 152 ng/g subsequent fluorination. However, Pu concentrations either stayed constant or decreased after the second fluorination (2 h reaction). This may be due to the formation of PuF_6 (gas); Scheele et al. [29] discusses the possibility of this volatile formation under high temperature and pressure conditions.

The Pu isotope ratios of UR and reacted Trinitite samples are displayed in Figure 11, and no clear trends are visible between measured ^{240}Pu/^{239}Pu ratios and fluorination time. For example, 4B 11.59 had a starting ^{240}Pu/^{239}Pu ratio = 0.0368, decreased to ^{240}Pu/^{239}Pu = 0.0203 after the 1 hr reaction, and ended with a similar ratio as the UR sample after the 2 h reaction (Figure 11). This is likely due to the weak ion signals measured for this sample with the lowest intensities for ^{239,240}Pu (1876 and 368 cps for the 1 h reaction, respectively). However, almost all of the measured ^{240}Pu/^{239}Pu ratios for the samples investigated here fall within the range of 'supergrade' Trinity Pu isotope signatures reported in the literature (represented as dashed lines; Figure 11), which indicates that Pu isotopes are not fractionating during the fluorination process, as expected.

5 Conclusions

This study demonstrates that the NF_3 thermal treatment can be a valuable tool for Si-based sample digestion in applications of forensic data mining. The NF_3 thermal treatment successfully (and rapidly) removes Si from minerals, glasses, and more importantly, Trinitite samples. This reaction leaves behind nonvolatile elements of interest (e. g. Cu, Pb, Pu, U) for nuclear forensic analysis. Due to the removal of Si from the glass, these elements are enriched (relative to the unreacted samples) and are therefore easier to identify; this feature is clearly demonstrated by both uranium and plutonium. Also, the measured Pu isotope ratios of reacted Trinitite samples match the 'supergrade' Trinity ^{240}Pu/^{239}Pu signature. Hence, the combined chemical and isotopic data reported here clearly indicate that NF_3 treatment of PDMs may significantly increase the likelihood of identifying the signature of bomb-related components, which provides a novel and more effective tool for source attribution purposes.

Acknowledgements: This work is funded by DOE/NNSA Grant PDP11-40/DE-NA0001112. We thank Dr. I. Steele and PNNL staff, S. M. Goodwin, B. J. Garcia, and A. D. Eckberg, for their guidance with electron microprobe analysis. We also thank J. Szymanowski for her guidance and training on PXRD analyses. Finally, we thank M. Schweiger and the staff at PNNL's Advanced Process Engineering Laboratory (APEL) for providing glass samples and sample preparation support.

References

1. Belloni, F., Himbert, J., Marzocchi, O., Romanello, V.: Investigating incorporation and distribution of radionuclides in trinitite. J. Environ. Radioactiv. **102**, 852 (2011).
2. Bellucci, J. J., Wallace, C., Koeman, E. C., Simonetti, A., Burns, P. C., Kieser, J., Port, E., Walczak, T.: Distribution and behavior of some radionuclides in the trinity nuclear Test. J. Radioanal. Nucl. Chem. **295**, 2049 (2013).
3. Bellucci, J. J., Simonetti, A., Wallace, C., Koeman, E. C., Burns, P. C.: Isotopic Fingerprinting of the World's First Nuclear Device Using Post-Detonation Materials. Anal. Chem. **85**, 4195 (2013).
4. Fahey, A. J., Zeissler, C. J., Newbury, D. E., Davis, J., Lindstrom, R. M. Postdetonation nuclear debris for attribution. Proc. Natl. Acad. Sci. **107**, 20207 (2010).
5. Parekh, P. P., Semkow, T. M., Torres, M. A., Haines, D. K., Cooper, J. M., Rosenberg, P. M., Kitto, M. E. (2006) Radioactivity in Trinitite six decades later. J. Environ. Radioactiv. **85**, 103 (2010).
6. Semkow, T. M., Parekh, P. P, Douglas, K. H.: Modeling the effects of the trinity test. In: T. M. Semkow, S. Pommé, S. M. Jerome (Eds.), Applied Modeling and Computations in Nuclear Science (2006), American Chemical Society, Washington, DC, vol. 943, p. 142.

7. Eby, N., Hermes, R., Charnley, N., Smoliga, J. A.: Trinitite – the atomic rock. Geol. Today **26**, 180 (2010).
8. Ross, C. S.: Optical properties of glass from Alamogordo, New Mexico. Am. Mineral. **33**, 360 (1948).
9. Wallace, C., Bellucci, J. J., Simonetti, A., Hainley, T., Koeman, E. C., Burns, P. C.: A multi-analytical approach for determination of radionuclide distribution in Trinitite. J. Radioanal. Nucl. Chem. **298**, 993 (2013).
10. Bellucci, J. J., Simonetti, A., Wallace, C., Koeman, E. C., Burns, P. C.: The Pb isotopic composition of Trinitite melt glass: evidence for the presence of Canadian industrial Pb in the first atomic weapon test. Anal. Chem. **85**, 7588 (2013).
11. Bellucci J. J., Simonetti A., Koeman E. C., Wallace C., Burns P. C.: A detailed geochemical investigation of post nuclear detonation Trinitite glass at high spatial resolution: delineating anthropogenic vs. natural components. Chem. Geol. **365**, 69 (2014).
12. Dustin, M. K., Koeman, E. C., Simonetti, A., Torrano, Z., Burns, P. C.: Comparative investigation between in-situ laser ablation- vs. bulk sample (Solution Mode)-ICP-MS Analysis of Trinitite post-detonation materials. Appl. Spectrosc. **70**, 1446 (2016).
13. Schmets, J. J.: Reprocessing of spent nuclear fuels by fluoride volatility processes. At. Energy Rev. **8**, 3 (1970).
14. Galkin, N. P., Ponomarev, L. A., Shishkov, Yu. D.: Investigation of processes of separation of uranium and plutonium hexafluorides. Radiokhimiya, **22**, 754 (1980).
15. Scheele R., McNamara, B. K., Casela, A. M., Kozelisky, A.: On the use of thermal NF_3 as the fluorination and oxidation agent in treatment of used nuclear fuels. J. Nucl. Mater. **424**, 224 (2012).
16. McNamara, B., Scheele, R., Kozelisky, A., Edwards, M.: Thermal reactions of uranium metal, UO_2, U_3O_8, UF_4, and UO_2F_2 with NF_3 to produce UF_6. J. Nucl. Mater. **394**, 166 (2009).
17. McNamara, B. K., Buck, E. C., Soderquist, C. Z., Smith, F. N., Mausolf, E. J., Scheele R. D.: Separation of metallic residues from the dissolution of a high-burnup BWR fuel using nitrogen trifluoride. J. Fluorine Chem. **162**, 1 (2014).
18. Neuerburg, G. J.: A method of mineral separation using hydrofluoric acid. Am. Mineral. **46**, 1498 (1961).
19. Golja, B., Barkanic, J., Hoff, A., Stach, J.: Plasma etching characteristics of Si and SiO_2 in NF_3/Ar and NF_3/He Plasmas. The Electrochem. Soc. Extended Abstracts (Washington, DC, October 9–14, 1983), pp. 207–208 (1983).
20. Barkanic, J. A., Reynolds, D. M., Jaccodine, R. J., Stenger, H. G., Parks, J., Vedage, V.: Plasma etching using NF_3: A review. J. Solid. State. Sci. Technol. **32**, 109 (1989).
21. Kastenmeier, B. E. E., Oehrlein, G. S., Langan, J. G., Entley, W. R.: Gas utilization in remote plasma cleaning and stripping applications. J. Vac. Sci. Technol. **18**, 2102 (2000).
22. Anderson, R. E., Vander Wall, E. M., Schaplowsky, R. K.: USAF propellant handbooks, vol. 3, Part A. Nitrogen Trifluoride, Systems Design Criteria, ADB028448, AeroJet Liquid Rocket Co, Sacramento, California (1978).
23. Borthwick, J., Harmon, R. S.: A note regarding CIF_3 as an alternative to BrF_5 for oxygen isotope analysis. Geochim. Cosmochim. Acta. **46**, 1665 (1982).
24. Jenner, G. A., Longerich, H. P., Jackson, S. E., Freyer, B. J.: ICP-MS – A powerful tool for high-precision trace-element analysis in Earth sciences: evidence from analysis of selected U.S.G.S reference samples. Chem. Geol. **83**, 133 (1990).
25. Chen, W., Simonetti, A.: In-situ determination of major and trace elements in calcite and apatite, and U-Pb ages of apatite from the Oka carbonatite complex: insights into a complex crystallization history. Chem. Geol. **353**, 151 (2013).
26. Donohue, P. H., Simonetti, A., Koeman, E. C., Mana, S., Burns, P. C.: Nuclear forensic applications involving high spatial resolution analysis of Trinitite cross-sections. J. Radioanal. Nucl. Chem. **306**, 457 (2015).
27. Bellucci, J. J., Simonetti, A.: Nuclear forensics: searching for nuclear device debris in trinitite-hosted inclusions. J. Radioanal. Nucl. Chem. **293**, 313 (2012).
28. Koeman, E. C., Simonetti, A., Burns, P. C.: Sourcing of copper and lead within red inclusions from Trinitite post-detonation material. Anal. Chem. **87**, 5380 (2015).
29. Scheele R. D., McNamara, B. K., Casela, A. M., Kozelisky, A. E., Neiner, D.: Thermal NF3 fluorination/oxidation of colbalt, yttrium, zirconium, and selected lanthanide oxides. J. Fluorine Chem. **146**, 86 (2013).
30. McDonough W. F., Sun S.-s.: The composition of the earth. Chem. Geol. **120**, 223 (1995).

Supplemental Material: The online version of this article (DOI: 10.1515/ract-2016-2641) offers supplementary material, available to authorized users.